Surface & Coatings Technology 251 (2014) 106–114

Contents lists available at ScienceDirect

Surface & Coatings Technology

journal homepage: www.elsevier.com/locate/surfcoat

Phase transformation in plasma electrolytic oxidation coatings on 6061 aluminum alloy

Vahid Dehnavi [a,*], Xing Yang Liu [b,1], Ben Li Luan [b,c,2], David W. Shoesmith [d,3], Sohrab Rohani [a,4]

[a] Department of Chemical and Biochemical Engineering, University of Western Ontario, London, ON N6A 5B9, Canada
[b] National Research Council Canada, 800 Collip Circle, London, ON N6G 4X8, Canada
[c] Department of Chemistry, University of Western Ontario, London, ON N6A 5B7, Canada
[d] Surface Science Western, Department of Chemistry, University of Western Ontario, London, ON N6A 5B7, Canada

ARTICLE INFO

Article history:
Received 12 February 2014
Accepted in revised form 5 April 2014
Available online 13 April 2014

Keywords:
Plasma electrolytic oxidation
Phase transformation
Alpha alumina
Gamma alumina
Electrical parameters

ABSTRACT

Oxide coatings were produced on a 6061 aluminum alloy using a pulsed unipolar plasma electrolytic oxidation (PEO) process. The effect of electrical parameters including pulse frequency, duty cycle and current density on phase formation in the coatings was revealed using conventional and glancing angle X-ray diffraction. The results show that PEO coatings are mainly composed of γ-Al_2O_3. Depending on the electrical parameters employed, the coatings can also contain α-Al_2O_3 and mullite with varying concentrations. Higher current densities and higher duty cycle were found to favor the formation of mullite. Under the experimental conditions used, the ratio of the integrated XRD peaks for α- and γ-Al_2O_3 varied from 0 to about 0.6, indicating that the relative content of α-Al_2O_3 in the PEO coatings varied over a wide range. Longer pulse on-times and higher current densities promoted the gamma to alpha-alumina phase transformation. Depth profiling of PEO ceramic coatings using glancing angle XRD with different incident beam angles revealed that mullite was more concentrated in the top surface of the coatings. No significant variation in α-Al_2O_3 concentration across the coatings could be concluded in this study, unlike the results of some other studies.

1. Introduction

Alumina ceramic coatings have great potential as hard, wear and corrosion resistant coatings on aluminum and its alloys. Various techniques including chemical vapor deposition (CVD), ionization-assisted magnetron sputtering PVD, and thermal spray are available to deposit alumina coatings, most of which involve high temperatures, but are not suitable for aluminum which has a relatively low melting point. As an alternative, coatings prepared by plasma electrolytic oxidation (PEO) are less expensive and easier to apply to components with complex geometries and large dimensions than the CVD, PVD or thermal spray processes [1,2]. PEO is a relatively new surface modification technique which can convert the surface of valve metals and alloys such as aluminum, magnesium, zirconium, and titanium into oxide ceramic coatings [3–6]. The PEO process involves complex chemical, electrochemical and plasma thermo-chemical reactions.

Despite extensive research, the mechanism of the PEO process is not comprehensively understood [7–9]. Hussein et al. [10] proposed a discharge model involving three distinct types of discharges, A, B, and C, for PEO on aluminum alloy substrates. Types A and C were thought to result from gas discharges occurring in micro-pores in the ceramic coating, and type B was attributed to dielectric breakdown through the oxide layer. More recently, an additional type of discharge has been proposed, type D, which occurs in large pores near the interface between the inner and outer layers [7]. These discharges play an essential role in the formation and properties of the resulting coatings, by influencing phase transformation, crystallization, annealing and sintering of the coating [11].

The PEO process involves multiple features. The characteristics of PEO coatings are affected by the compositions of the substrate material and the electrolyte, process parameters such as the current regime (AC, DC, and pulsed DC), current density, duty cycle, frequency and treatment time [12–14]. In addition to the type of current regime, the current polarity and application sequence could also affect the properties of the coatings. It is suggested that the pulsed bipolar current mode generally improves the properties of the PEO coatings and results in coatings with higher density [15]. In a study on a magnesium alloy substrate, it was found that applying a hybrid current mode, in which a unipolar current was applied first followed by a bipolar current, improved the coating properties in terms of microstructure and corrosion resistance [16].

* Corresponding author. Tel.: +1 519 702 5582.
E-mail addresses: vdehnavi@uwo.ca, vdehnavi@gmail.com (V. Dehnavi), XingYang.Liu@nrc-cnrc.gc.ca (X.Y. Liu), Ben.Luan@nrc-cnrc.gc.ca (B.L. Luan), dwshoesm@uwo.ca (D.W. Shoesmith), srohani@uwo.ca (S. Rohani).
[1] Tel.: +1 519 430 7042.
[2] Tel.: +1 519 430 7043.
[3] Tel.: +1 519 661 2111x86366.
[4] Tel.: +1 519 661 4116.

http://dx.doi.org/10.1016/j.surfcoat.2014.04.010
0257-8972/

PEO coatings produced on aluminum alloy substrates in dilute silicate electrolytes are mainly composed of α- and γ-Al_2O_3 with some amorphous alumina. In electrolytes with a high concentration of silicate, mullite is also observed [1,7,17–19]. Thick coatings, with high mullite content, possess good thermal and chemical stability and are good candidates for thermal barrier applications [2,20].

PEO coatings have also been reported to have superior wear and corrosion resistance compared to untreated aluminum alloy substrates [1,14]. The hardness of the PEO coating is a function of the nature of the dominant phases present, as well as their ratio and distribution and the porosity and density of micro-cracks in the coatings. The hardness of alumina phases have been reported to be around 26 GPa for α-Al_2O_3, 17 GPa for γ-Al_2O_3, 10.5 GPa for mullite, and 7 GPa for the amorphous anodically formed alumina. However, the measured hardness in PEO coatings is lower than in dense bulk alumina due to porosity in PEO coatings [7,11,20]. Tribological studies indicate coatings composed of α-Al_2O_3 show a higher wear resistance [21].

It is believed that increasing the α-Al_2O_3 content will enhance the wear performance of PEO coatings [22,23]. This improved hardness compared to conventional coatings formed by anodization is attributed to the presence of a large proportion of crystalline material, namely α- and γ-Al_2O_3, and to a reduced porosity [24]. Controlling the α-Al_2O_3 content of the coating, which is the hardest phase among alumina phases, is a very interesting topic in PEO studies which may prove advantageous in producing coatings with higher hardness. There are a few studies in which some aspects of the phase transformation of coatings during PEO treatment on aluminum alloy substrates have been investigated, but the phenomenon is far from being well understood. Khan et al. [25] found a decreased duty cycle caused a corresponding decrease in the ratio of α- to γ-Al_2O_3 in PEO coatings on 6082 aluminum alloy produced by pulsed unipolar current, although large data scatter was observed. Xue et al. [17] investigated the phase distribution of ceramic coatings on 2024 aluminum alloy and concluded that the surface layer of coatings mainly contained γ-Al_2O_3 and the percentage of α-Al_2O_3 gradually increased from the external surface towards the inner layers of the coatings. Applying higher current densities [11,12,26] and increasing the deposition time which resulted in thicker coatings [21,27] were reported to increase the α-Al_2O_3 content in the coatings.

Hard PEO coatings mainly composed of α-Al_2O_3 could be a promising candidate to protect Al alloy substrates against wear. Here, we report possible procedures to control the α-Al_2O_3 content in alumina oxide coatings by varying the electrical parameters in the PEO process. The results of the current study provide a reference for the possible industrial applications of PEO coatings where a high hardness is required.

2. Material and methods

2.1. Sample preparation

Disk specimens were cut from a 6061 aluminum alloy bar with an average diameter of 30 mm and an average thickness of 8 mm. The specimens were then ground with 600 grit SiC paper, degreased in propanol and rinsed with distilled water. Electrical contact to specimens was made using a steel rod bolted to a threaded hole drilled in the side of each specimen.

2.2. Coating process

PEO coatings were produced using a custom built, unipolar pulsed DC source in an electrolyte containing 2 g/L Na_2SiO_3 + 2 g/L KOH in deionized water. Samples served as the anode and were submerged in the electrolyte in a stainless steel tank which also served as the counter cathode. During the PEO process, the electrolyte temperature was maintained below 40 °C by circulating the electrolyte through an external heat exchanger. To investigate the effect of electrical parameters on phase transformations in the coatings, two frequencies, 50 and 1000 Hz, at duty cycles of 20% and 80% with current densities (J) of 5, 10, 15, 20, and 25 A/dm^2 were used. The samples were coated under galvanostatic conditions, i.e. the current was kept constant during the entire process and the anode potential was allowed to vary. All samples were coated for 30 min. Table 1 lists the sample codes with the corresponding electrical conditions used.

During a single pulse, t_{on} and t_{off} are the periods during which the current is on and off, respectively, and the duty cycle (D_t) is defined by Eq. (1).

$$D_t = \left[t_{on}/\left(t_{on} + t_{off}\right)\right] \times 100 \quad (1)$$

The waveform and corresponding parameters of the unipolar pulsed power source are given in Fig. 1.

2.3. Coating characterization

The surface morphologies of the PEO coatings were examined using a Hitachi S-3500N scanning electron microscope (SEM). The samples were sputter-coated with gold prior to SEM examination to minimize surface charging. A Philips X'Pert_MRD diffractometer with Cu Kα (40 kV and 40 mA) radiation was used to study the composition of the coatings. The samples were scanned over the 2θ range from 15° to 90° with a 0.02° step size. To determine the distribution of different crystalline phases throughout the coating, and to minimize interference from the aluminum substrate, glancing angle XRD at incidence angles of 1, 2.5 and 5° was performed to supplement conventional (Bragg–Brentano configuration) X-ray diffraction measurements. Coating thickness was measured using an Eddy current gauge.

3. Results and discussion

3.1. Coating surface morphology and thickness

SEM micrographs of four samples showing the typical surface morphology of PEO coatings are presented in Fig. 2. Almost all samples contain two different kinds of regions: cratered regions with a central hole and lighter areas with a nodular structure. Craters are formed when molten material is ejected from the coating/substrate interface through central holes due to the high temperatures and strong electric field present during the PEO process. On contact with the electrolyte, the molten material solidifies rapidly [28].

Previously [13] the cratered regions were shown to be rich in aluminum while the nodular structures exhibited a higher concentration of Si compared to Al. Changing the electrical parameters, namely the duty cycle and frequency, was found to alter the size of the craters and also the ratio of the craters to the nodular structures on the sample surface.

The thicknesses of coatings prepared by PEO using different electrical parameters are presented in Fig. 3. For each set, the thickness of the PEO coating increases with increasing current density as a result of the increased energy input. For samples PEO coated at 1000 Hz, the difference in the thickness of the samples processed at the same current density but different duty cycles is insignificant; however, the average thickness of each sample coated at a duty cycle of 20% is slightly greater

Table 1
Electrical parameters and sample codes for PEO treatment on 6061 Al alloy.

Sample code	Frequency (Hz)	Duty cycle, D_t (%)	t_{on} (ms)	t_{off} (ms)	*: J (A/dm^2)
S12-*	1000	20	0.2	0.8	5, 10, 15,
S18-*	1000	80	0.8	0.2	20, 25
S52-*	50	20	4	16	
S58-*	50	80	16	4	

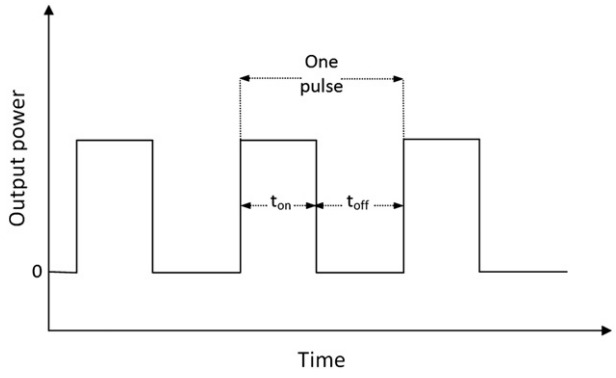

Fig. 1. Schematic of the pulsed unipolar output of a plasma electrolytic oxidation power supply (t_{on}: pulse on time; t_{off}: pulse off time).

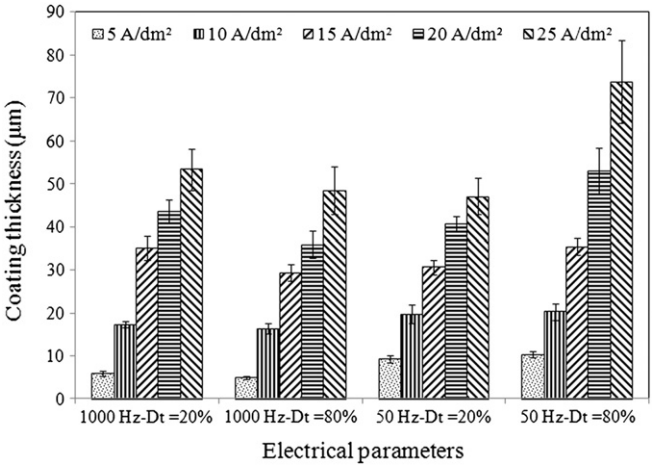

Fig. 3. Effect of electrical parameters on coating thickness of PEO treated 6061 aluminum alloy substrates.

than the sample coated at the same current density but a duty cycle of 80%.

It should be pointed out that the coating measurements performed do not consider the porosity of the coatings. Studies [29] show that PEO coatings contain fine networks of channels, formed by localized electrical discharges, and pores due to the entrapment of gases formed during the process in the molten alumina. The shorter the t_{on} time, the more the possibility of gases trapped inside the coating, resulting in coatings possibly of higher porosity. The slightly higher thickness readings of samples S12-* compared to samples S18-* could be linked to the higher porosity level in these samples.

For samples coated at 50 Hz and current densities of 5, 10, and 15 A/dm^2, variation of the duty cycle did not cause a significant change in the coating thickness. Samples S58-20 and S58-25, however, showed considerably higher thicknesses compared to all other samples. The reason for this could be linked to the increased concentration of Si-rich species on the outer surface of the coatings on these samples and is discussed later in Sections 3.3 and 3.4. The results suggest that frequency does not have a significant effect on the coating thickness variation of samples produced at the same current density.

3.2. Coating phase analysis

Examples of the XRD patterns obtained using conventional X-ray diffraction for coatings produced at a current density of 20 A/dm^2 are presented in Fig. 4. Studying the XRD patterns of all samples revealed that the coatings were mainly composed of γ-Al_2O_3. In addition, in some samples, α-Al_2O_3 (S18-20, S52-20, and S58-20) and mullite (S58-20) were also observed.

Alpha alumina is a stable alumina phase with a high melting point (2050 °C) and possesses the corundum structure consisting of oxygen anions in hexagonal close-packed layers with cations occupying octahedral sites. Gamma alumina is a metastable phase which consists of layers of cubic close-packed oxygen anions with cations in the octahedral and tetrahedral sites [24,30]. It can transform to α-Al_2O_3 upon heating in the temperature range 800 to 1200 °C [22,31,32]. The phase transformation temperature can be affected by factors such as

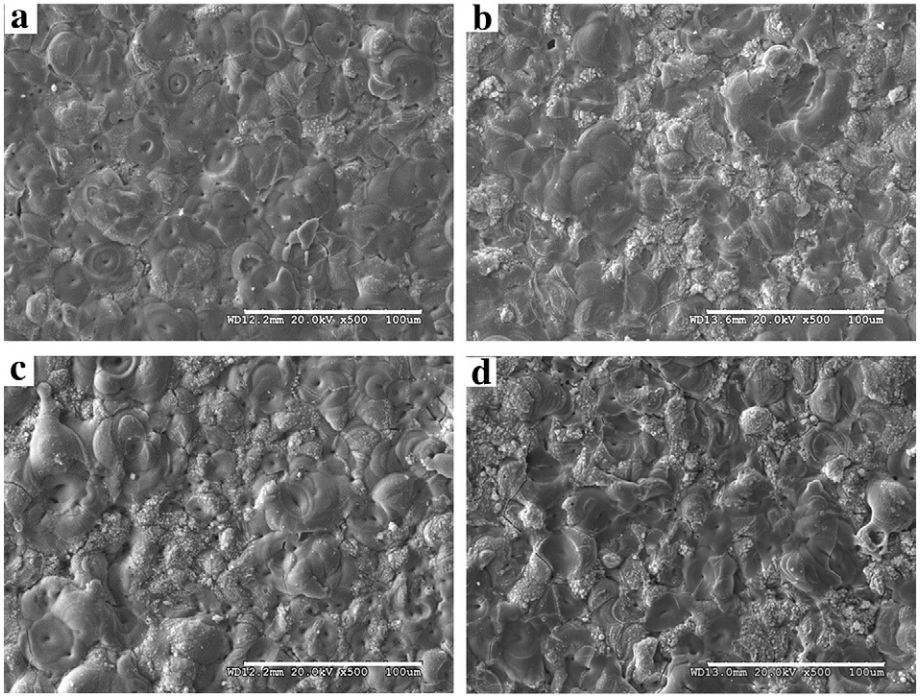

Fig. 2. SEM images (secondary electron mode) of free surface of PEO coatings on samples (a) S12-10, (b) S18-10, (c) S52-10 and (d) S58-10.

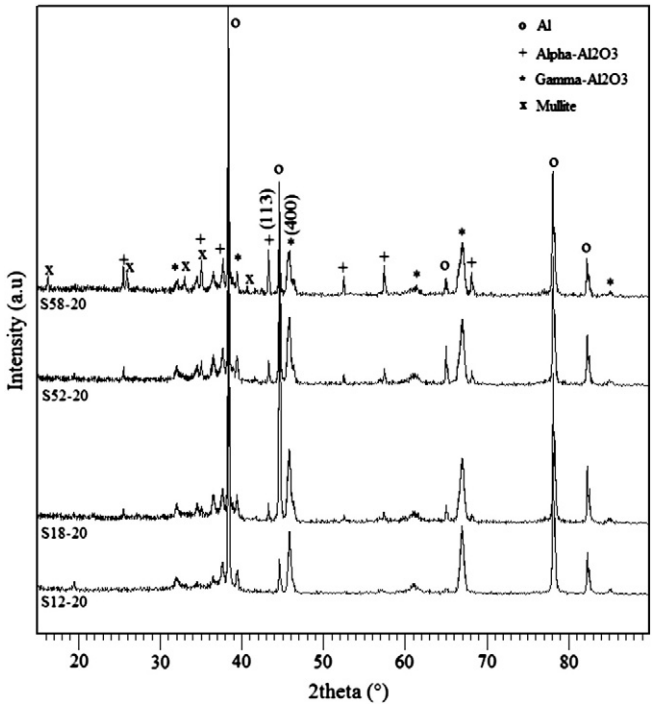

Fig. 4. X-ray diffraction patterns (Bragg–Brentano configuration) of PEO ceramic coatings on samples S12-20, S18-20, S52-20, and S58-20 formed at $J = 20$ A/dm^2.

atmospheric conditions, the processing method used, and the presence of impurities in the alumina [33,34]. Schaper et al. [24] studied the phase transformation of gamma to alpha alumina quantitatively using high temperature differential thermal analysis (DTA) and observed an exothermic peak in all DTA curves in the temperature range 1100–1200 °C, which corresponds to the γ-$Al_2O_3 \rightarrow \alpha$-$Al_2O_3$ phase transformation. Cava et al. [35] investigated the phase transition in alumina nanopowders using XRD and micro-Raman spectroscopy and observed that it occurred in the temperature range 950–1050 °C.

3.3. Influence of electrical parameters on the phase content of coatings

XRD patterns obtained using glancing angle XRD with an incident beam angle of 5° are presented in Figs. 5 and 6. Glancing angle XRD greatly enhances the analysis of coatings by reducing interference from the sample substrate and increasing the path of the incident beam within the coating layer itself.

Comparison of the four sets of XRD spectra in Figs. 5 and 6 shows that the intensities of Al diffraction peaks at each frequency and duty cycle decrease with increasing current density. Al diffraction peaks are from the substrate and increasing the current density results in a thicker coating. This was confirmed by coating thickness measurements, with the thickness of the coatings varying from a minimum of about 5 μm for sample S18-5 to above 70 μm for sample S58-25 (Fig. 3). When glancing angle XRD is used, the path length of the incident beam through the coating is increased and the XRD patterns confirm that the coating mainly consists of γ-Al_2O_3 with various contents of α-Al_2O_3.

Coatings on samples treated at a frequency of 1000 Hz and a duty cycle of 20% with different current densities (Fig. 5-a) contain mainly γ-Al_2O_3, while samples treated at the same frequency but a duty cycle of 80% (Fig. 5-b) show the presence of α-Al_2O_3 peaks in addition to γ-Al_2O_3 at current densities of 15, 20 and 25 A/dm^2.

For samples treated at a lower frequency of 50 Hz and a duty cycle of 20% (Fig. 6-a), the coating, at a current density of 5 A/dm^2 (S52-5), is mainly composed of γ-Al_2O_3 while for samples coated at higher current densities, α-Al_2O_3 peaks are also observed. A similar phase distribution was obtained on samples treated at the same frequency but a duty cycle of 80%. For both duty cycles the intensity of α-Al_2O_3 peaks increased when the current density was raised from 10 to 25 A/dm^2 indicating an increase in α-Al_2O_3 content in the coating.

Table 2 summarizes the identified phases in the PEO coatings formed using different electrical parameters. As can be seen in Table 2, samples treated at current densities of 20 and 25 A/dm^2 at 50 Hz and a duty cycle of 80% contain mullite in addition to α- and γ-Al_2O_3, while samples treated at 1000 Hz contain no detectable mullite.

Mullite ($3Al_2O_3 \cdot 2SiO_2$) is composed of aluminum, oxygen and silicon and is the only stable phase in the Al_2O_3–SiO_2 binary system at atmospheric pressure. Mullite formation occurs at temperatures above

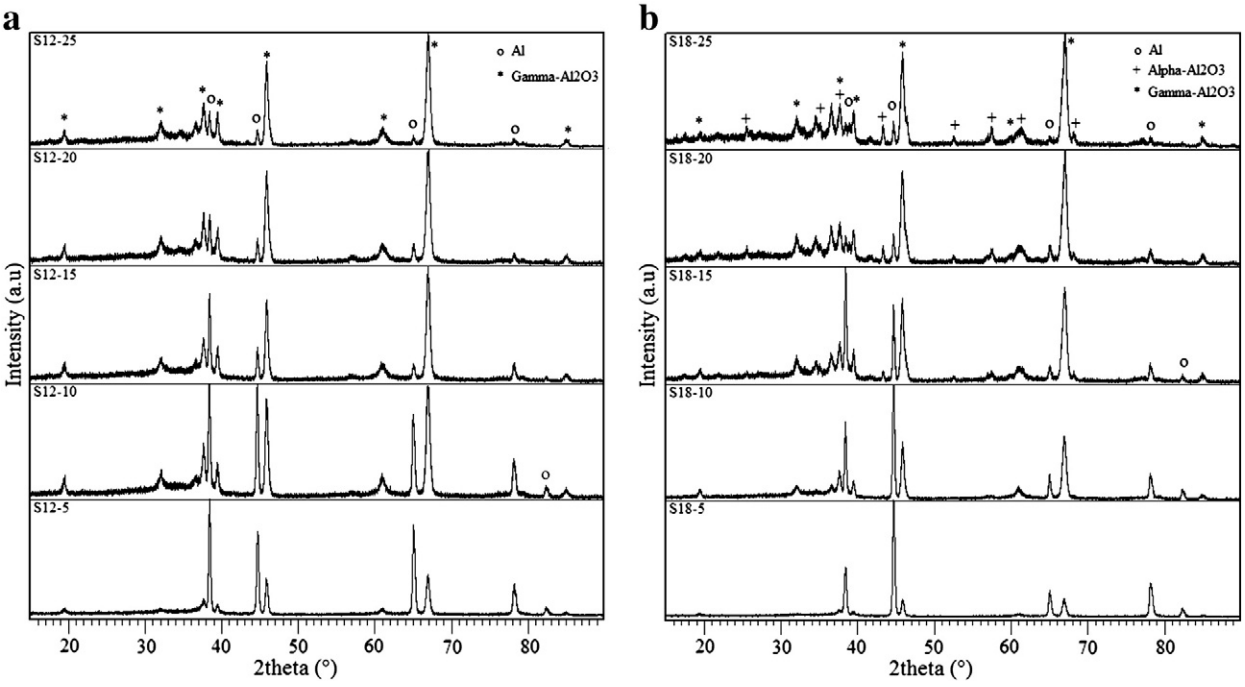

Fig. 5. Glancing angle XRD (incident angle of 5°) of samples PEO coated at a frequency of 1000 Hz and duty cycles of (a) 20% and (b) 80%.

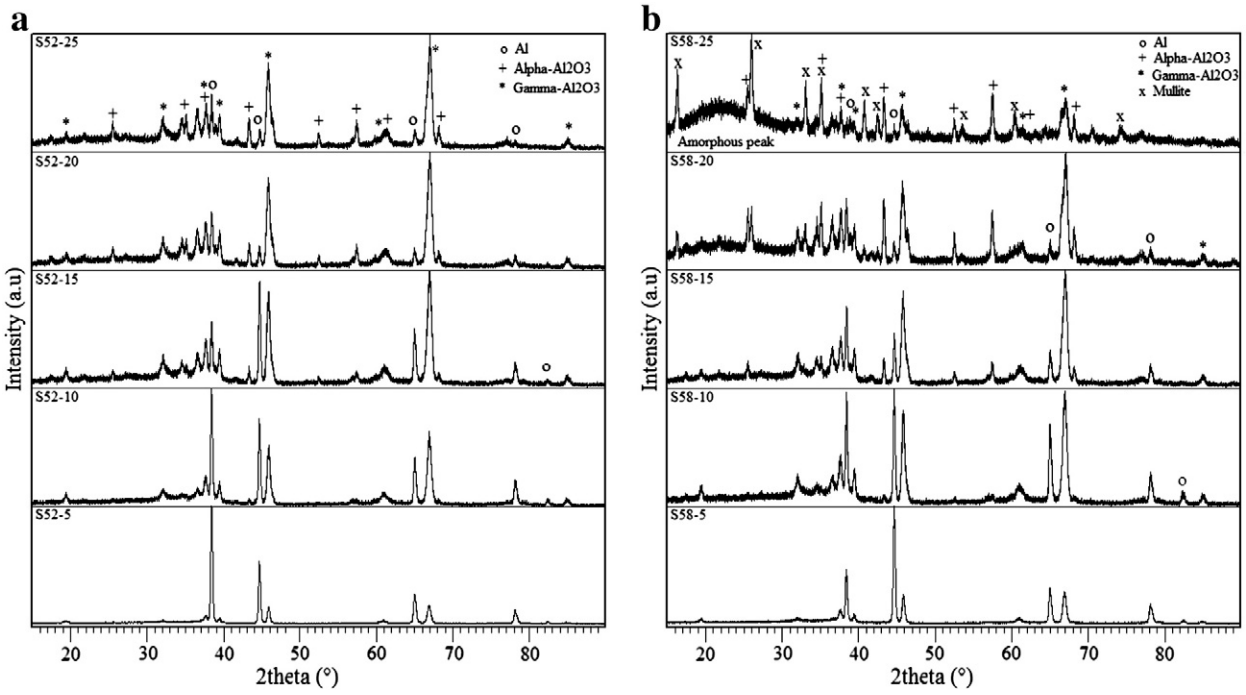

Fig. 6. Glancing angle XRD (incident angle of 5°) of samples PEO coated at a frequency of 50 Hz and duty cycles of (a) 20% and (b) 80%.

1000 °C depending on the processing route employed, possibly by a nucleation and growth mechanism involving reaction between Al_2O_3 and SiO_2 [36–38]. It is generally assumed that increasing the concentration of sodium silicate in the electrolyte enhances the formation of mullite in the coatings [2,20]. A previous study [13] shows that the duty cycle and frequency affect the surface morphology, the micro-discharge characteristics, and the distribution of elements in the coatings. Lower duty cycles were found to result in micro-discharges with higher intensities but lower spatial density. Al/Si ratios calculated from surface EDX elemental maps showed that the concentration of Si increased on the surface of the coated samples when the current frequency was decreased and the duty cycle increased. For the same frequencies, samples treated at a duty cycle of 80% contained more Si on the surface than those treated at a duty cycle of 20%. Comparing the free surface SEM images (Fig. 2) of the samples treated at the same frequency but different duty cycles confirms this fact. In sample S12-10 (Fig. 2-a), treated at a frequency of 1000 Hz and a duty cycle of 20%, the surface is mainly composed of craters which were previously shown to be rich in Al. However, sample S18-10 (Fig. 2-b) treated at the same frequency but a duty cycle of 80% contains patches of lighter areas previously shown to be rich in Si [13].

Mullite was detected only in samples S58-20 and S58-25, which were treated at a frequency of 50 Hz and duty cycle of 80%. This could be linked to the increased concentration of Si on the surface of these samples. As mentioned earlier, mullite forms by reaction between Al_2O_3 and SiO_2 and in samples coated at 50 Hz and a high duty cycle of 80%, Si concentration is higher as compared to 1000 Hz.

The relative contents of α-Al_2O_3 and γ-Al_2O_3 phases were estimated on the basis of the integrated intensities of the $(113)_\alpha$ and $(400)_\gamma$ peaks (I_α and I_γ, respectively), (Fig. 4). The integrated intensity ratio of the two peaks, I_α/I_γ, was used as an indicator of the approximate relative amounts of the two phases in the coatings. The possible effect of the involvement of the Al substrate peaks on the results will be discussed later in Section 3.4.

Table 2
Phase contents of the coatings on 6061 aluminum alloy samples PEO treated using different electrical parameters.

Frequency (Hz)	Duty cycle, D_t (%)	J (A/dm^2)	Main phases in the coating
1000	20	5	γ
		10	γ
		15	γ
		20	γ
		25	γ, little α
	80	5	γ
		10	γ, little α
		15	γ, α
		20	γ, α
		25	γ, α
50	20	5	γ
		10	γ, α
		15	γ, α
		20	γ, α
		25	γ, α
	80	5	γ
		10	γ, α
		15	γ, α
		20	γ, α, mullite, amorphous phase
		25	γ, α, mullite, amorphous phase

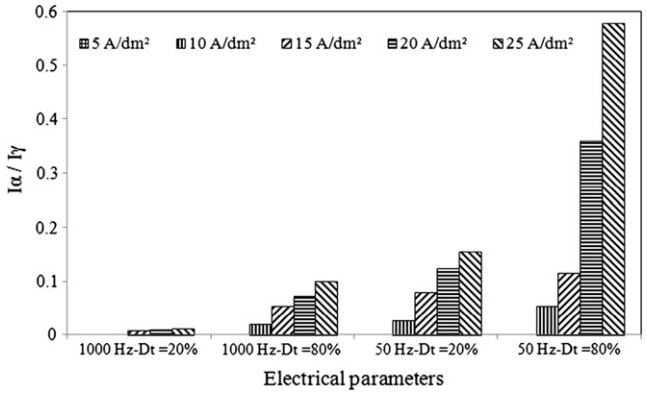

Fig. 7. Influence of electrical parameters on the relative content of α-Al_2O_3 in PEO coatings on 6061 aluminum alloy.

The $(113)_\alpha$ and $(400)_\gamma$ peaks have strong intensities and can be used as the characteristic peaks for α-Al_2O_3 and γ-Al_2O_3, respectively. The interplanar distances of the $(113)_\alpha$ and $(400)_\gamma$ planes are similar (2.085 Å and 1.977 Å, respectively). The diffraction angles of the two peaks are close but clearly separated and do not overlap with other peaks [17,27]. A similar approach was also used by Hsu et al. [39], Wu et al. [12], Guangliang et al. [26], Khan et al. [11] and Gu et al. [31].

Fig. 7 shows that I_α/I_γ varied in a range from 0 to about 0.6, indicating that the relative contents of α-Al_2O_3 to γ-Al_2O_3 varied depending on the electrical parameters employed during the PEO treatment.

It has been suggested that solidification of molten alumina at considerable undercoolings results in the formation of γ-Al_2O_3 rather than α-Al_2O_3 because the critical free energy of nucleation for γ-Al_2O_3 is lower [18,40]. For γ-Al_2O_3 to transform to α-Al_2O_3 both cation and anion rearrangement are required and this transformation occurs only at high temperatures. It is known that the γ-Al_2O_3 → α-Al_2O_3 transformation proceeds through a series of transition phases (δ- and θ-$A1_2O_3$) which leads to stable α-Al_2O_3 at room temperature. γ, δ and θ-$A1_2O_3$ are believed to be similar in structure with oxygen ions in a cubic close-packed arrangement and cations occupying different available octahedral and tetrahedral sites. Since these intermediate structures are similar to γ-$A1_2O_3$, the series of transitions can be conveniently represented as a single phase transformation of the γ-Al_2O_3 → α-Al_2O_3 [24,40–42].

Steiner et al. [41] studied the kinetics of the γ-Al_2O_3 → α-Al_2O_3 transformation in the temperature range of 1050 to 1200 °C and observed that the higher the temperature, the faster the transformation. It has been proposed that this transformation proceeds via a nucleation and growth mechanism with the kinetics obeying the Kolmogorov–Johnson–Mehl–Avrami (KJMA) equation (Eq. (2)),

$$C_\alpha = 1 - \exp(-kt^n) \tag{2}$$

where C_α is the fraction of the α-Al_2O_3 formed, k is the temperature-dependent rate constant (s^{-1}), t is time (s), and n is the Avrami exponent [24,33,43].

By substituting properly estimated values for the parameters in the KJMA equation, it is possible to explain the variation in α-Al_2O_3 content with the different electrical parameters. According to Eq. (2), increasing the values of k and t will result in an increase in C_α providing n is positive. Macedo et al. [33] obtained a nearly constant value for the Avrami exponent ($n = 2.1$) for different isotherms and values for the rate constant (k) for different constant temperatures in the range 700 to 1200 °C are available [33,43]. By substituting plausible values of k, n and t in Eq. (2), it is possible to estimate the kinetics of the γ-Al_2O_3 → α-Al_2O_3 phase transformation as a function of the electrical parameters.

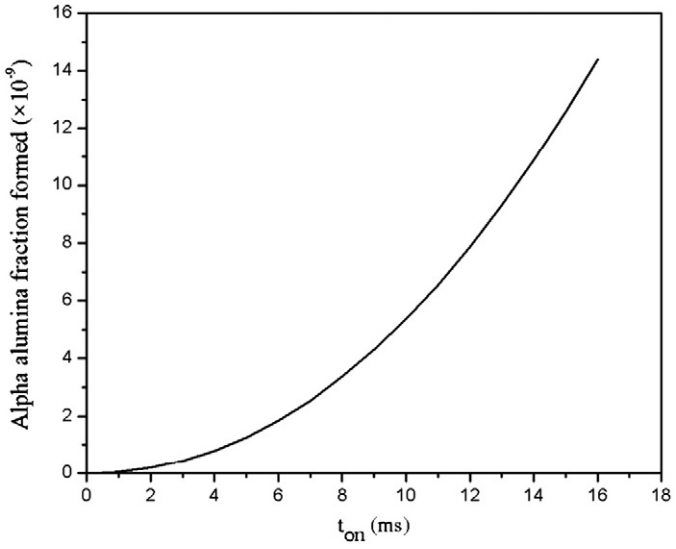

Fig. 8. Variation trend in the fraction of formed α-alumina in a single pulse as a function of t_{on} calculated using KJMA equation assuming an isothermal transformation temperature of 1050 °C.

Setting t equal to t_{on} (Table 1), i.e., the pulse on-time during PEO treatment, n equal to 2.1 and assuming that the phase transition occurs isothermally at 1050 °C and with a value of k equal to 8.5×10^{-5} s^{-1} (the value at 1050 °C [43]), yields a value of the α-Al_2O_3 fraction formed in a single pulse. Fig. 8 shows how this fraction varies for pulse on-times between the shortest and the longest pulse on-times of 0.2 and 16 ms corresponding to sample series S12 and S58, respectively.

Increasing the pulse on-time from 0.2 to 16 ms results in an exponential increase in the fraction of γ-Al_2O_3 transformed to α-Al_2O_3, Fig. 8. The pulse on-time increases for each of the groups of data shown from left to right (0.2, 0.8, 4 and 16 ms) in Fig. 7. For each specific current density, the integrated peak intensity ratio of $(113)_\alpha$ and $(400)_\gamma$, (I_α/I_γ), also increases from left to right, consistent with the trend observed in Fig. 8. This explains why at a frequency of 1000 Hz and a duty cycle of 20% very little α-Al_2O_3 is formed only at high current densities of 20 and 25 A/dm^2. At short pulse on-times, there is insufficient time for the rearrangement of anions and cations required for the γ → α-Al_2O_3 phase transformation. It should be noted that, while this rationale is consistent with observations, the final fraction of α-Al_2O_3 formed depends on the interaction of a number of factors including the total duration of pulse on-time, the intensity and energy of micro-discharges, and the annealing effect of the subsequent micro-discharges on the already formed solid oxide layers. The γ-Al_2O_3 formed early in the PEO process could transform to α-Al_2O_3 as a result of the heat generated in the coating by subsequent through-thickness discharges [20].

During PEO, the sparking intensity depends on the energy of each pulse and the single pulse energy increases when using higher current density. The single pulse energy (E_p) is defined as:

$$E_p = \int_0^{(t_{on})} U_p \cdot I_p dt \tag{3}$$

where U_p is the pulse voltage, I_p is the pulse current and t_{on} is the pulse on time [15]. This increase in pulse energy would explain why increasing the current density increases the α-Al_2O_3 fraction formed for each set of samples with the same frequency and duty cycle. Also, it can be deduced from Fig. 7 that, regardless of the frequency and duty cycle employed, a current density of 5 A/dm^2 does not produce the conditions required for the γ → α-Al_2O_3 phase transformation. This could possibly be attributed to two factors: a current density of 5 A/dm^2 did not produce micro-discharges with sufficient energy to provide the heat necessary for the phase transformation, and the thinner coating thickness (<10 μm) created at low current densities (Fig. 3) led to faster heat conduction into the aluminum substrate, and hence made it more difficult to achieve the temperature required for the γ → α-Al_2O_3 transformation.

3.4. Depth profiling of ceramic coatings

The X-ray spectra of samples S52-20 and S58-20 obtained at glancing angles of 1, 2.5, and 5° are compared with the conventional XRD (Bragg–Brentano configuration) spectra in Fig. 9-a and b, respectively. It is observed that sample S58-20, treated at a higher duty cycle, contains mullite in addition to α- and γ-Al_2O_3. By varying the glancing angle it is possible to depth profile the surface layers. By comparing the mullite peak intensities to those of the other phases at different glancing angles in Fig. 9-b, it can be inferred that mullite is more concentrated near the surface of the coatings since its peak intensities decrease relative to those of the other phases when the incident beam angle is increased from 1 to 5°.

Changing the electrical parameters affects the micro-discharge characteristics. Increasing the duty cycle and lowering the frequency

generates micro-discharges with lower spatial density but higher intensity which results in higher concentrations of Si rich species on the surface of the coatings [13,44]. This increased Si concentration facilitates the formation of mullite ($3Al_2O_3 \cdot 2SiO_2$). Moreover, glancing angle XRD patterns of samples S58-20 (Fig. 9-b) and S58-25 (Fig. 6-b) show the presence of an additional amorphous phase ($2\theta = 15–30$). An amorphous peak at a similar 2θ position has been observed by others [2,20,45–47]. This amorphous phase cannot be easily distinguished in the conventional XRD patterns, Fig. 4, due to the strong peak intensities for the other phases. The intensity of this peak decreases with an increase in glancing angle from 1 to 5°, suggesting that it is located at the outer surface of the coatings. In addition to the formation of mullite, deposition of Si rich species on the coating surface could contribute to the coating thickness. Samples S58-20 and 58-25 have considerably thicker coatings compared to other samples prepared at the same current densities, Fig. 3, which could be linked to the deposition of Si rich species on the surface of these samples. As discussed earlier, at later stages of the PEO coating process, microdischarge behavior changes and microdischarges tend to become more intense with less spatial density. This change is more readily noticeable at lower frequencies and higher duty cycles. The results of the previous studies [15,46] suggest that silicon-rich species form a gel which deposits on the coating surface. For samples S58-20 and S58-25, the decreased spatial density of microdischarges increases the chance of the Si-rich deposits to stay on the surface since the ejection of the Si-rich deposits by microdischarges will act on a relatively smaller portion of the surface area.

The literature on the distribution of different phases across the PEO coatings is inconsistent. It has been reported [14,17] that the amount of α-Al_2O_3 gradually increases from the top surface towards the substrate-coating interface. Xue et al. [18] observed that the α-Al_2O_3 content gradually increases from the surface layer towards the interior of the coating but reached a maximum at ~50 μm from the coating/substrate interface before decreasing near the interface. Others [14,22] have reported that the α-Al_2O_3 content increased gradually with increasing coating thickness.

To investigate the distribution of the α-Al_2O_3 phase across the coatings, the integrated intensity ratio of $(113)_\alpha$ and $(400)_\gamma$ peaks (I_α/I_γ) was calculated for each sample using the XRD patterns obtained by conventional XRD (Bragg–Brentano configuration) and different glancing angles and the results were compared. The I_α/I_γ values for samples treated at a current density of 15 A/dm^2 are compared in Table 3. No significant differences were observed when comparing I_α/I_γ values of different samples calculated using the XRD spectra with different glancing angles. This implies that no α-Al_2O_3 concentration gradient occurs through the coatings. These results are at odds with studies [14,17] in which the α- and γ-Al_2O_3 phase distribution at different coating depths were determined by polishing the coating to a certain thickness and then performing XRD analysis.

It has been suggested [14,22] that the α-Al_2O_3 content increases gradually as the PEO coating thickens. However, using short pulse t_{on} times, it was observed [44] that varying the coating thickness from 10 to ~80 μm by employing longer deposition times did not create any α-Al_2O_3, and only mullite was identified in addition to γ-Al_2O_3 at longer deposition times. The rearrangement of oxygen anions and aluminum cations, necessary during the γ-$Al_2O_3 \rightarrow \alpha$-$Al_2O_3$ phase transition, occurs via diffusion which is a function of time and temperature. However, alumina has a relatively low thermal conductivity [2], and the dominance of γ-Al_2O_3 in thinner coatings can be attributed to the higher cooling rates which favor the formation of γ-Al_2O_3. In thicker coatings, on the other hand, the thermal energy can accumulate in the coatings leading to the higher temperatures required to promote the $\gamma \rightarrow \alpha$-$Al_2O_3$ phase transition [14,22,40]. However, the effect of time should not be neglected since it plays an important role in diffusion processes. Previously [48], it was observed that in the PEO coatings prepared at a current density of 15 A/dm^2, decreasing the pulse t_{on} times below 0.2 ms resulted in no α-Al_2O_3 formation during coating growth.

In this study, the relative contents of α- and γ-Al_2O_3 phases in the PEO coatings were estimated using the relative peak intensity ratios of $(113)_\alpha$ and $(400)_\gamma$ and the Al substrate was not involved in the calculations. The reason for this is that $(200)_{Al}$ peak, located at 2θ angle of 44.72° (JCPDS 1-085-1327), is clearly separated and does not overlap with either $(113)_\alpha$ peak located at 2θ angle of 43.36° (JCPDS 10-0173), or $(400)_\gamma$ peak located at 2θ angle of 45.86° (JCPDS 10-0425), as can be seen in Fig. 4. The integrated intensity ratios (I_α/I_γ) calculated

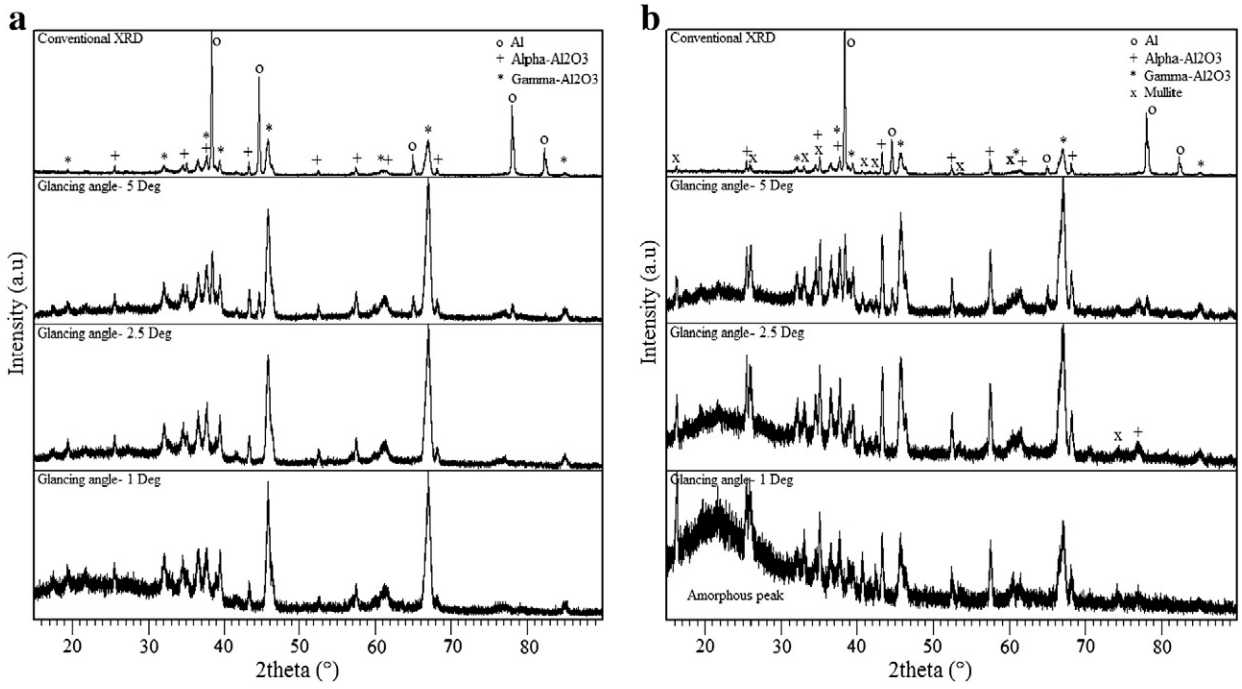

Fig. 9. XRD patterns of samples (a) S52-20 and (b) S58-20 at glancing angles of 1, 2.5 and 5° vs. the conventional XRD (Bragg–Brentano configuration) pattern.

Table 3
The integrated intensity ratios of $(113)_\alpha$ and $(400)_\gamma$ peaks (I_α/I_γ) calculated at different XRD conditions.

Sample XRD condition	S12-15 I_α/I_γ	S18-15 I_α/I_γ	S52-15 I_α/I_γ	S58-15 I_α/I_γ
Glancing angle, 1°	0	0.06	0.06	0.16
Glancing angle, 2.5°	0	0.05	0.08	0.14
Glancing angle, 5°	0.01	0.06	0.08	0.12
Conventional XRD	0	0.08	0.09	0.13

using different XRD conditions, in which the contribution of the aluminum substrate might vary, suggested that excluding the Al substrate did not have a significant impact on the results. Table 3 lists I_α/I_γ values calculated for samples coated at a current density of 15 A/dm^2 as an example. Similar results were obtained for other samples as well. As can be observed in Table 3, although the X-ray beam penetration depth, and as a result, the contribution from the Al substrate in the total XRD pattern of the samples varied when different XRD conditions (conventional XRD, glancing XRD with incident beam angles of 1, 2.5 and 5°) were applied, the obtained I_α/I_γ values for each sample at different XRD conditions were very similar.

4. Conclusions

Samples of 6061 aluminum alloy were PEO treated in an alkaline silicate electrolyte using a pulsed unipolar current regime. Two different frequencies of 50 and 1000 Hz and duty cycles of 20% and 80% were employed at a number of current densities of 5, 10, 15, 20, and 25 A/dm^2. The effect of electrical parameters on phase composition, transformation, and distribution was examined using conventional (Bragg–Brentano configuration) and glancing angle XRD. The following conclusions can be drawn from this study:

(1) Phase distribution and composition, including the α-Al_2O_3 to γ-Al_2O_3 ratio, in the PEO coatings can be controlled by using different electrical conditions.
(2) PEO coatings produced on 6061 Al alloys are mainly composed of γ-Al_2O_3. The relative content of α-Al_2O_3 in the coatings changed by varying the electrical parameters. Depending on the electrical parameters employed, various amounts of mullite and an amorphous phase were identified. Alpha-Al_2O_3 represents the hardest form of alumina and is believed to enhance the wear resistance of PEO coatings.
(3) Coatings on samples PEO treated at a frequency of 1000 Hz and a duty cycle of 20% with different current densities contained essentially only γ-Al_2O_3. Increasing the duty cycle to 80% at the same frequency resulted in the formation of α-Al_2O_3 in addition to γ-Al_2O_3. In samples treated at 50 Hz, α-Al_2O_3 was identified in all samples at a current density greater than 5 A/dm^2 in addition to γ-Al_2O_3. Some mullite was also detected in these samples plus an amorphous phase in samples treated at high current densities of 20 and 25 A/dm^2 and a duty cycle of 80%.
(4) It was found that increasing the pulse on-time by employing a lower frequency and higher duty cycle enhanced the $\gamma \rightarrow \alpha$-$Al_2O_3$ phase transformation. The results were consistent with the trend predicted by the Kolmogorov–Johnson–Mehl–Avrami (KJMA) equation which describes the kinetics of mechanisms involving nucleation and growth.
(5) Formation of mullite in samples treated at lower frequency was linked to the microdischarge behavior. Increasing the duty cycle and lowering the frequency generate microdischarges with lower spatial density but higher intensity which results in higher concentrations of Si rich species on the surface of the PEO coatings. Increased Si concentration facilitates the formation of mullite.
(6) Depth profiling of ceramic coatings using glancing angle XRD showed no significant variation in α-Al_2O_3 concentration across the coatings.

Conflict of interest

None.

Acknowledgments

This research was supported by National Research Council Canada (NRC), Ontario Graduate Scholarship (OGS), and Natural Science and Engineering Research Council of Canada (NSERC) grants. The authors would like to acknowledge David Arnold for helping with XRD analysis and Dr. Yang Song, of Chemistry Department at the University of Western Ontario, for his comments on XRD.

References

[1] X. Nie, E.I. Meletis, J.C. Jiang, A. Leyland, A.L. Yerokhin, A. Matthews, Surf. Coat. Technol. 149 (2002) 245–251.
[2] J.A. Curran, H. Kalkancı, Y. Magurova, T.W. Clyne, Surf. Coat. Technol. 201 (2007) 8683–8687.
[3] S. Dejiu, C. Jingrui, L. Guolong, H. Donglei, W. Lailei, M. Haojie, et al., Vacuum 99 (2014) 143–148.
[4] E. Matykina, A. Berkani, P. Skeldon, G.E. Thompson, Electrochim. Acta 53 (2007) 1987–1994.
[5] S. Wang, Y. Xia, L. Liu, N. Si, Ceram. Int. 40 (2014) 93–99.
[6] Y. Cheng, F. Wu, E. Matykina, P. Skeldon, G.E.E. Thompson, Corros. Sci. 59 (2012) 307–315.
[7] Y. Cheng, Z. Xue, Q. Wang, X.-Q. Wu, E. Matykina, P. Skeldon, et al., Electrochim. Acta 107 (2013) 358–378.
[8] R.C. Barik, J.A. Wharton, R.J.K. Wood, K.R. Stokes, R.L. Jones, Surf. Coat. Technol. 199 (2005) 158–167.
[9] L.O. Snizhko, A. Yerokhin, N.L. Gurevina, D.O. Misnyankin, A.V. Ciba, A. Matthews, Surf. Coat. Technol. 205 (2010) 1527–1531.
[10] R.O. Hussein, D.O. Northwood, X. Nie, J. Vac. Sci. Technol. A 28 (2010) 766–773.
[11] R.H.U. Khan, A. Yerokhin, X. Li, H. Dong, A. Matthews, Surf. Coat. Technol. 205 (2010) 1679–1688.
[12] H. Wu, J. Wang, B.B. Long, Z. Jin, W. Naidan, F. Yu, et al., Appl. Surf. Sci. 252 (2005) 1545–1552.
[13] V. Dehnavi, B.L. Luan, D.W. Shoesmith, X.Y. Liu, S. Rohani, Surf. Coat. Technol. 226 (2013) 100–107.
[14] T. Wei, F. Yan, J. Tian, J. Alloys Compd. 389 (2005) 169–176.
[15] B.L. Jiang, Y.M. Wang, in: H. Dong (Ed.), Surf. Eng. Light Alloy. Aluminum, Magnes. Titan. Alloy., Woodhead Publishing, 2010, pp. 110–153.
[16] R.O. Hussein, D.O. Northwood, X. Nie, J. Alloys Compd. 541 (2012) 41–48.
[17] W. Xue, Z. Deng, Y. Lai, R. Chen, J. Am. Ceram. Soc. 81 (1998) 1365–1368.
[18] W. Xue, Z. Deng, R. Chen, T. Zhang, H. Ma, J. Mater. Sci. 36 (2001) 2615–2619.
[19] L.R. Krishna, A.S. Purnima, G. Sundararajan, Wear 261 (2006) 1095–1101.
[20] H. Kalkancı, S.C. Kurnaz, Surf. Coat. Technol. 203 (2008) 15–22.
[21] J. Tian, Z. Luo, S. Qi, X. Sun, Surf. Coat. Technol. 154 (2002) 1–7.
[22] H.-H. Wu, Z.-S. Jin, B.-Y. Long, F.-R. Yu, X.-Y. Lu, Chin. Phys. Lett. 20 (2003) 1815–1818.
[23] W. Xue, Z. Deng, R. Chen, T. Zhang, Thin Solid Films 372 (2000) 114–117.
[24] H. Schaper, L.L. Van Reijen, Thermochim. Acta 77 (1984) 383–393.
[25] R.H.U. Khan, A.L. Yerokhin, T. Pilkington, A. Leyland, A. Matthews, Surf. Coat. Technol. 200 (2005) 1580–1586.
[26] Y. Guangliang, L. Xianyi, B. Yizhen, C. Haifeng, J. Zengsun, J. Alloys Compd. 345 (2002) 196–200.
[27] A.L. Yerokhin, L.O. Snizhko, N.L. Gurevina, A. Leyland, A. Pilkington, A. Matthews, J. Phys. D. Appl. Phys. 36 (2003) 2110–2120.
[28] G. Sundararajan, L. Rama Krishna, Surf. Coat. Technol. 167 (2003) 269–277.
[29] J.A. Curran, T.W. Clyne, Acta Mater. 54 (2006) 1985–1993.
[30] G. Lv, W. Gu, H. Chen, W. Feng, M.L. Khosa, L. Li, et al., Appl. Surf. Sci. 253 (2006) 2947–2952.
[31] W.-C. Gu, G.-H. Lv, H. Chen, G.-L. Chen, W.-R. Feng, G.-L. Zhang, et al., J. Mater. Process. Technol. 182 (2007) 28–33.
[32] M. Bodaghi, A.R. Mirhabibi, H. Zolfonun, M. Tahriri, M. Karimi, Phase Transit. 81 (2008) 571–580.
[33] M.I.F. Macêdo, C.A. Bertran, C.C. Osawa, J. Mater. Sci. 42 (2007) 2830–2836.
[34] C.-K. Loong, J.W. Richardson Jr., M. Ozawa, J. Alloys Compd. 250 (1997) 356–359.
[35] S. Cava, S.M. Tebcherani, I.A. Souza, S.A. Pianaro, C.A. Paskocimas, E. Longo, et al., Mater. Chem. Phys. 103 (2007) 394–399.
[36] S. Sembiring, W. Simanjuntak, Makara J. Sci. 16/2 (2012) 77–82.
[37] C. Gerardin, S. Sundaresan, J. Benziger, A. Navrotsky, Chem. Mater. 6 (1994) 160–170.
[38] M.A. Sainz, F.J. Serrano, J.M. Amigo, J. Bastida, A. Caballero, J. Eur. Ceram. Soc. 20 (2000) 403–412.
[39] C.-H. Hsu, H.-P. Teng, F.-H. Lu, Surf. Coat. Technol. 205 (2011) 3677–3682.
[40] R. McPherson, J. Mater. Sci. 8 (1973) 851–858.
[41] C.J.-P. Steiner, D.P.H. Hasselman, R.M. Spriggs, J. Am. Ceram. Soc. 54 (1971) 412–413.
[42] R. Damani, P. Makroczy, J. Eur. Ceram. Soc. 20 (2000) 867–888.
[43] R.A. Shelleman, G.L. Messing, M. Kumagai, J. Non-Cryst. Solids 82 (1986) 277–285.

[44] V. Dehnavi, B. Luan, X.Y. Liu, D.W. Shoesmith, S. Rohani, Mater. Sci. Technol., Montreal, Canada, 2013, pp. 2247–2254.
[45] M. Tarakci, Mater. Charact. 62 (2011) 1214–1221.
[46] F. Monfort, A. Berkani, E. Matykina, P. Skeldon, G.E. Thompson, H. Habazaki, et al., Corros. Sci. 49 (2007) 672–693.
[47] T. Abdulla, A. Yerokhin, R. Goodall, Mater. Des. 32 (2011) 3742–3749.
[48] V. Dehnavi, X.Y. Liu, B. Luan, S. Rohani, D.W. Shoesmith, Int. Conf. Mater. Heat Treat. ICMH 2012, Isfahan, Iran, 2012.